Macromolecules

pubs.acs.org/Macromolecules Article

Thermodynamically Originated Stacking Fault in the Close-Packed Structure of Block Copolymer Micelles

Li-Ting Chen, Yu-Ting Huang, Chun-Yu Chen, Meng-Zhe Chen, and Hsin-Lung Chen*

Cite This: *Macromolecules* 2021, 54, 8936–8945 Read Online

ACCESS | Metrics & More | Article Recommendations | Supporting Information

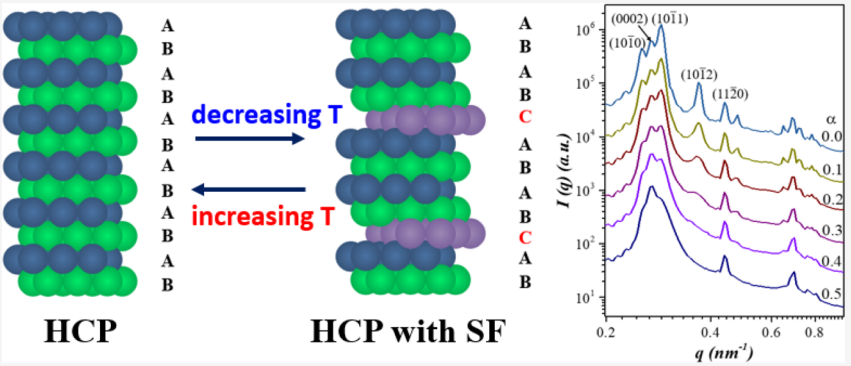

ABSTRACT: Stacking faults of hexagonal close-packed layers (HCPLs) often exist as kinetically trapped defects in the close-packed lattices of metallic atoms and spherical colloidal particles. Here, we show that the population of stacking faults in the hexagonal close-packed (HCP) lattice of the micelles formed by the blends of poly(ethylene oxide)-*block*-poly(1,4-butadiene) (PEO-*b*-PB) with PEO or PB homopolymer increased with decreasing temperature in a thermally reversible manner. We argue that, while HCP is the equilibrium lattice for a close-packed micellar phase with an infinitely large grain, introduction of stacking faults becomes thermodynamically favored when the lateral dimension of the HCPL and the difference in the bulk free energy between face-centered cubic (FCC) and HCP lattices are small. An optimal degree of stacking fault exists in the close-packed structure under the balance between the bulk lattice free energy and an entropic gain from the combinatorial mixing of FCC and HCP layers in the stacking direction. The higher extent of stacking faults at lower temperature found in the present system was attributed to the smaller difference in the bulk free energy between FCC and HCP lattices, which further signified that the micelles packed in the HCP lattice have higher entropy than those organized in the FCC phase.

INTRODUCTION

Colloidal particles with narrow size distribution undergo a first-order transition from the liquid phase to the crystalline phase above a critical particle concentration governed by the nature and range of interparticle interaction. For hard spherical particles displaying hard-sphere potential, crystallization is driven purely by entropy and the spheres tend to organize into a close-packed lattice that provides more free volume for the particles to explore than random close packing.[1] Face-centered cubic (FCC) and hexagonal close-packed (HCP) are the two types of close-packed lattices constructed by the close stacking of the hexagonal close-packed layers (HCPLs) in ABCABC... and ABABAB... sequences, respectively.[2] Here, A denotes the position of the reference HCPL, and the positions of B and C layers are obtained by a translation of $\mathbf{a}/3 + 2\mathbf{b}/3$ and $2\mathbf{a}/3 + \mathbf{b}/3$ relative to A, respectively, with **a** and **b** being the hexagonal lattice vectors in the layers. In spite of having the same particle packing fraction of 0.74, hard spheres organized in an FCC lattice possess slightly higher positional entropy in an amount of $10^{-3}k_B$ per particle than those packed in an HCP lattice; consequently, FCC has been regarded as the thermodynamically stable close-packed lattice of a hard-sphere crystal.[3−5]

Micelles formed by a block copolymer (bcp) in the melt state and in the selective solvents with the corresponding homopolymer or a foreign solvent constitute a class of soft colloid that also organizes into long-range ordered lattices. Unlike the hard-sphere colloids devoid of any internal structure, a bcp micelle contains a core and a corona composed of the two types of block chains. The soft coronas of bcp micelles tend to fill the space homogeneously, leading to deformation of the micelles into polyhedra called "Voronoi

Received: April 12, 2021
Revised: August 22, 2021
Published: September 21, 2021

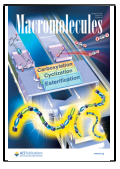

https://doi.org/10.1021/acs.macromol.1c00792
Macromolecules 2021, 54, 8936–8945

cells" with their geometry determined by the packing lattice.[6,7] Entropy also plays a crucial role in selecting the stable lattice of bcp micelles, but it is the conformational entropy of the block chains instead of the positional entropy of the micelles that usually dominates the selection.[6,7] Provided that the core adopts spherical geometry and the coronal blocks are confined within the Voronoi cell, body-centered cubic (BCC) is the favored packing structure of bcp micelles, in which the truncated octahedron Voronoi cell of the BCC lattice has higher sphericity than the rhombic dodecahedron cells of the close-packed lattices and hence offers lower packing frustration arising from the non-uniform deformation of the coronal blocks for space filling.[7,8]

BCC is indeed the predominantly observed lattice structure of bcp micelles, while other packing symmetries including close-packed lattices[9−19] and Frank−Kasper phases[8,20−30] have also been disclosed under certain conditions. Recently, we have shown that, in a narrow phase window wherein the close-packed structure is stable, HCP was favored over FCC for the micelles composed of pure bcp molecules[17] as well as those formed by bcp/homopolymer blends with the homopolymer dissolved selectively in the coronal region.[16] These findings attest a generic difference between soft colloid and hard colloid in selecting their stable close-packed lattices.

FCC and HCP are the two close-packed structures with completely regular stacking of HCPLs and are thus characterized by well-defined space groups. Nevertheless, the only requirement for close packing is that the adjacent HCPLs, i.e., i and $i + 1$, have different positions. Attaining perfect FCC or HCP packing would hence require the coherent interaction beyond the nearest neighbors, that is, the "communication" between layers i and $i + 2$ to assure that they have a different (for FCC) or identical (for HCP) position.[31] The presence of an HCPL with a faulty sequence in an HCP or FCC lattice is called a "stacking fault".[31−37] The extent of the stacking fault can be represented by the probability α that layers i and $i + 2$ have different positions, as defined by Pusey *et al.*[31,36] Thus, $\alpha = 0$ and 1 correspond to perfect HCP and FCC packing, respectively, and $\alpha = 0.5$ represents random hexagonal close packing (r-HCP) comprising completely random stacking sequences of HCPLs, such as ···ABCBCACB···.

The better thermodynamic stability of FCC relative to HCP and r-HCP for a hard-sphere crystal has been established using computer simulation.[3−5,33] Mau and Huse further showed the higher stability of FCC relative to all possible stacking sequences with $\alpha \neq 1$.[5] Nevertheless, due to a very small difference in free energy among different stacking sequences, a hard-sphere system may be easily trapped into metastable close-packed structures other than pure FCC.[31,33,36] Moreover, Auer and Frenkel have revealed that r-HCP is more stable than FCC in the early stage of nucleation where the crystal size is still small; as a result, the crystallization of hard spheres could proceed via Ostwald's step rule with r-HCP as the precursory structure followed by growing into FCC crystals.[38] The metastable r-HCP phase has indeed been observed frequently in the freshly grown colloidal crystals, which then transformed slowly to FCC packing via prolonged aging.[33,34,36] The r-HCP phase has also been identified during the growth of the ordered phase of block copolymer micelles toward the thermodynamically stable FCC phase.[39]

In a previous study of micelle packing in the blends of a bcp, poly(ethylene oxide)-*block*-poly(1,4-butadiene) (PEO-*b*-PB), with a PB or PEO homopolymer (denoted as h-PB and h-PEO, respectively), we found that the ordering of the micelles composed of PEO (or PB) blocks forming the core and the coronas containing the wet brush mixture of PB (or PEO) blocks with the corresponding homopolymers proceeded through a rather complex pathway.[16] The crystallization of PEO blocks in the solvent casting process for blend preparation destroyed the micellar structure. The micellar entity recovered upon heating above the melting point of PEO crystals and was found to organize in the r-HCP phase. The random stacking of HCPLs tended to regulate into the regular sequence of FCC packing with further heating, and an order−disorder transition transforming the ordered phase to a micellar liquid phase eventually took place. In the subsequent cooling process from the micellar liquid phase, the micelles organized into an HCP lattice rather than an FCC lattice. Since the initial solvent history was erased upon accessing the micellar liquid phase, the HCP phase thus developed was considered to be equilibrium in nature. In this study, we reveal an even more complex mechanism underlying the micelle ordering process, which involves a monotonic variation of the degree of stacking fault in the HCP phase with temperature. We will show that the randomness of the close stacking of HCPLs increased with decreasing temperature, and the trend of variation was thermally reversible. We argue that, though HCP is the equilibrium lattice for the close-packed micellar phase with an infinitely large grain, the introduction of stacking faults is thermodynamically favored when the lateral dimension of the HCPL and the bulk free-energy difference between the HCP and FCC phases are small. Under this condition, the combinatorial entropy of mixing between FCC and HCP layers that favors the r-HCP structure becomes significant and its competition with the bulk lattice free energy that favors perfect HCP packing leads to an optimal degree of stacking fault in the close-packed structure.

EXPERIMENTAL SECTION

Materials and Blend Preparation. The PEO-*b*-PB sample was acquired from Polymer Source, Inc. Its number average molecular weights (M_n) and the polydispersity index (PDI) determined by gel permeation chromatography (GPC) were 12,800 g/mol and 1.04 (see Figure S1 of the Supporting Information), respectively, which agreed well with those provided by the manufacturer. The molecular weights of PEO and PB blocks deduced from ^{1}H nuclear magnetic resonance (NMR) spectroscopy (see Figure S2 of the Supporting Information) and the total molecular weight were 5300 and 7500 g/mol, respectively, which also agreed well with those provided by the manufacturer.

The h-PB with $M_n = 1.0 \times 10^3$ g/mol (PDI = 1.10) and the h-PEO with $M_n = 1.5 \times 10^3$ g/mol (PDI = 1.09) were also obtained from Polymer Source, Inc. The blends with the overall volume fractions of PEO (f_{PEO}) of 0.2 and 0.83 (or $f_{PB} = 0.17$) were prepared by blending the PEO-*b*-PB with h-PB and h-PEO, respectively, via solvent casting. The PEO-*b*-PB and the homopolymers were first dissolved in toluene at room temperature followed by drying in vacuo at 60 °C for 4 h to obtain the solvent-cast blends. The detailed information of the blend compositions is displayed in Table S1 of the Supporting Information.

Small-Angle X-ray Scattering (SAXS) Measurements. Temperature-dependent SAXS measurements were conducted at beamline BL23A1 of the National Synchrotron Radiation Research Center (NSRRC), Hsinchu, Taiwan. The energy of the employed monochromatic radiation was 15 keV, prescribing an X-ray wavelength of 0.83 Å. The 2D scattering patterns were collected with a PILATUS 1 M detector. The measured magnitude of the scattering wave vector q ranged from 0.07 to 4 nm^{-1} ($q = (4\pi/\lambda)\sin(\theta/2)$, where θ is the scattering angle and λ is the wavelength). All the

https://doi.org/10.1021/acs.macromol.1c00792
Macromolecules 2021, 54, 8936−8945

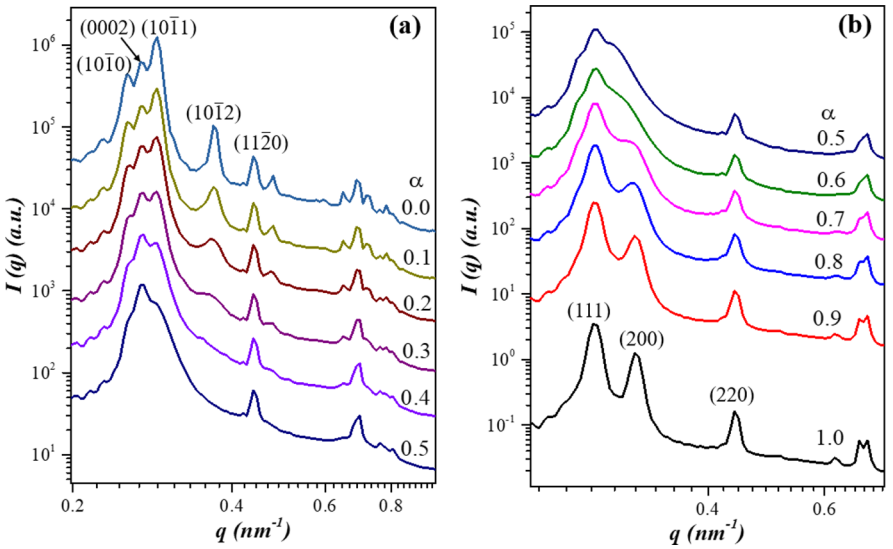

Figure 1. Calculated SAXS profiles of the close-packed structures of 20 layers of HCPL with different values of α in (a) the HCP regime ($\alpha \leq 0.5$) and (b) the FCC regime ($\alpha \geq 0.5$). The lateral dimension of the HCPL was set as N_p = 400 particles, and the close-stacking distance between the HCPLs and the radius of the spherical core domain were 23.2 and 8.2 nm, respectively. The (10$\bar{1}$2) and (200) peaks in the HCP and FCC regimes, respectively, are particularly sensitive to the change in the degree of stacking fault, where their intensity and breadth decreased with increasing fault probability.

scattering profiles were corrected for the scatterings from air and an empty cell. The temperature ramping rate was about 5 °C/min, and the sample was allowed to equilibrate at each temperature for 5 min followed by data acquisition for 1 min. All SAXS measurements were conducted under a nitrogen atmosphere, which effectively circumvented the occurrence of degradation and a cross-linking reaction, as verified by GPC and ^{1}H NMR spectroscopy measurements for the copolymer sample after subjecting it to the thermal cycles involved in the temperature-dependent SAXS measurement. The temperature-dependent SAXS experiments were repeated four times using different batches of each blend composition to assure the reproducibility of the experimental results.

RESULTS AND DISCUSSION

The SAXS Profiles of the Close-Packed Micellar Phase Containing Stacking Faults. The close-packed structure is formed by the close stacking of HCPLs with the positions denoted by A, B, and C. Here, we calculated the SAXS patterns of the close stacking of N_L layers of the HCPL associated with the assigned values of α by the Debye equation after the real-space model was constructed.[16] To establish the real-space model, we first assigned a value of α; the computer program then generated two HCPLs, each composed of N_p 2D hexagonally packed mass points (corresponding to the centers of the spherical micelles), in AB stacking. The position of the third layer may be A or C with the probability weighting according to the assigned value of α. To assign the position of the third layer, the program selected a random number x from the uniform distribution over the range $0 \leq x \leq 1$. If x was smaller than or equal to α, the position of the third layer was different from that of the first layer, that is, it was assigned as C. If x was larger than α, the third layer was assigned as A. The positions of the subsequent layers were assigned by the same protocol till the total N_L layers were generated.

The lattice factor $S(q)$ of the close-stacked HCPLs thus constructed was calculated by the Debye equation:[41]

$$S(q) = \sum_i \sum_j \frac{\sin(q|\mathbf{r}_i - \mathbf{r}_j|)}{q|\mathbf{r}_i - \mathbf{r}_j|} \quad (1)$$

where $\mathbf{r}_i$ and $\mathbf{r}_j$ stand for the positions of the mass points in the lattice, and the summation in eq 1 was carried out over all mass points building up the close-packed structure. Once $S(q)$ was obtained, the scattering intensity was calculated by multiplying $S(q)$ with the form factor $P(q,R_c)$ of the monodisperse spherical core of the micelle with a designated core radius R_c, viz., $I(q) = KS(q)P(q,R_c)$, where K is a proportionality constant. The calculation was performed for 100 times to yield the average SAXS curve associated with the designated α value.

Figure 1 shows the calculated SAXS profiles of the close-packed structures of 20 layers of HCPL with different values of α. The lateral dimension of the HCPL was set as N_p = 400 particles, and the close-stacking distance between the HCPLs and R_c were 23.2 and 8.2 nm, respectively. The small ripples observed at q < 0.24 nm^{-1} arose from the finite grain size assumed in the calculation; therefore, only the scattering features at q > 0.24 nm^{-1} were considered. The variation of the scattering pattern with α displayed in Figure 1 was similar to that reported by Martelozzo *et al.* in a study of the transformation of the metastable r-HCP to the FCC structure in a hard-sphere crystal during the aging process.[36] Figure 1a shows the variation of the SAXS pattern with α in the "HCP regime" with $\alpha \leq 0.5$, where $(AB)_{N_L/2}$ was the perfect stacking sequence with α = 0. Figure 1b presents the calculated SAXS curves in the "FCC regime" with $\alpha \geq 0.5$, where $(ABC)_{N_L/3}$ was the perfect stacking sequence with α = 1.

In the HCP regime, the perfect HCP lattice with α = 0 exhibits the diffraction peaks with the position ratio of 1:1.06:1.13:1.46:1.73··· associated with the (10$\bar{1}$0), (0002), (10$\bar{1}$1), (10$\bar{1}$2), (11$\bar{2}$0)··· diffractions, respectively. As the probability of the stacking fault (or α) increased, all peaks at q < 0.6 nm^{-1} were found to diminish and broaden except the (0002) and (11$\bar{2}$0) peaks. The (10$\bar{1}$2) peak was particularly

https://doi.org/10.1021/acs.macromol.1c00792
Macromolecules 2021, 54, 8936−8945

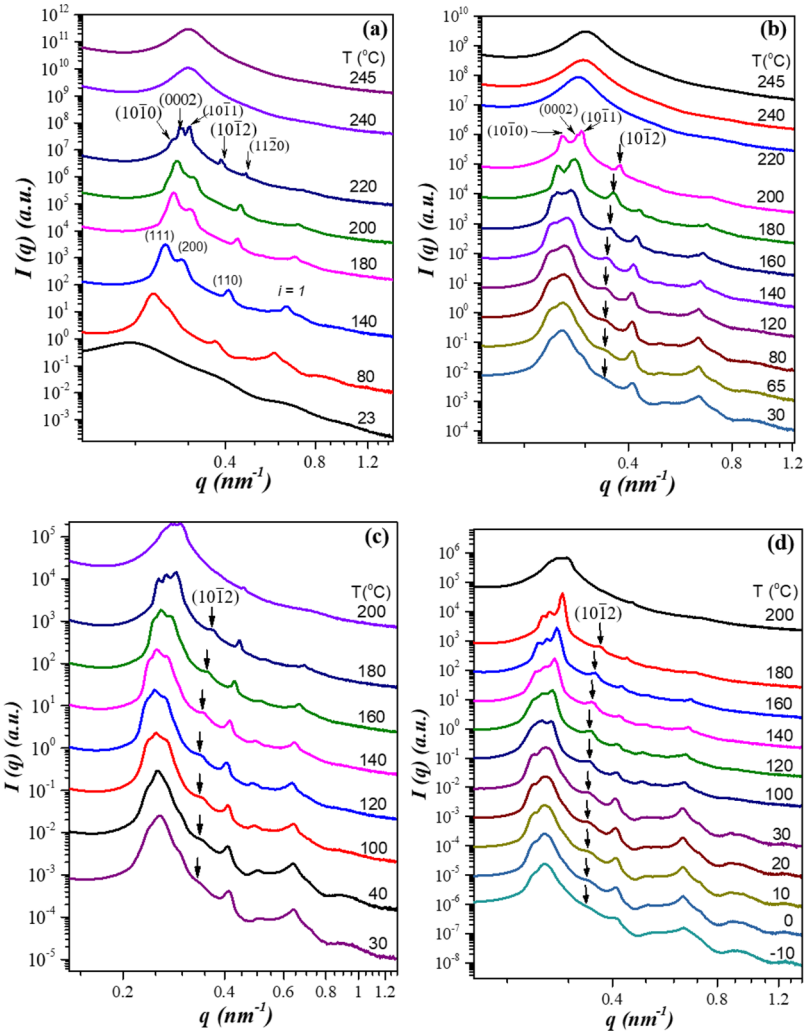

Figure 2. Temperature-dependent SAXS profiles of PEO-*b*-PB/h-PB blend (f_{PEO} = 0.20) collected in (a) the first heating, (b) subsequent cooling, (c) reheating, and (d) recooling cycle. The (10$\bar{1}$2) peak observed in (b) to (d) diminished and broadened progressively with decreasing temperature, indicating an increase in the degree of stacking fault in the HCP regime. The peak denoted as "i = 1" in (a) corresponds to the first-order form factor maximum of the PEO core domain.

sensitive to the degree of stacking fault, as the increase in α from 0 to 0.2 caused a strong depression and broadening of this peak, while the perturbation of the first three peaks was less evident. Consequently, the (10$\bar{1}$2) peak was utilized here to examine the change in the degree of stacking fault in the HCP regime.

In the FCC regime, the perfect FCC lattice with α = 1 exhibits the diffraction peaks with the position ratio of $1:(4/3)^{1/2}:(8/3)^{1/2}:(11/3)^{1/2}:(12/3)^{1/2}$, corresponding to the (111), (200), (220), (311), and (222) diffractions, respectively. The increase in the degree of stacking fault (or decrease of α) led to clear diminishment and broadening of the (200) peak; this peak can thus be employed to evaluate the degree of stacking fault in the FCC regime. The calculated scattering curve of the r-HCP phase (α = 0.5) shows a sharp primary peak and a broad hump beside it.

The SAXS Results of PEO-*b*-PB/Homopolymer Blends Showing the Temperature-Dependent Degree of Stacking Fault. Figure 2a–d presents the SAXS profiles of the PEO-*b*-PB/h-PB blend with f_{PEO} = 0.2 collected in the first heating (from the as-cast state), subsequent cooling, reheating, and recooling cycles, respectively. As seen in Figure 2a, the SAXS profile at 30 °C (i.e., the onset of heating from the solvent-cast blend) showed rather featureless broad peaks arising from the distorted morphology generated by the crystallization of PEO blocks in the solvent casting process. Upon melting the PEO crystals at 80 °C, the corresponding SAXS profile showed the feature of the FCC phase with a high degree of stacking fault, as the (200) peak was very broad. The (200) peak sharpened with a further increase in temperature, indicating the reduction of the extent of the stacking fault in the FCC lattice. Nevertheless, the FCC phase transformed into HCP when the temperature was increased to 220 °C. The (10$\bar{1}$2) peak associated with the HCP phase thus formed was sharp, indicating a limited degree of stacking fault. It is noted that the (0002) peak was stronger than the (10$\bar{1}$1) peak due to the large number of close-stacked layers (i.e., N_L) along the stacking direction relative to the lateral size of HCPL determined by N_p in the HCP lattice. This was demonstrated in Figure S3 of the Supporting Information showing the calculated SAXS curves of the HCP phase with systematic variations of N_p and N_L. The HCP phase transformed into the micellar liquid phase upon heating to 240 °C.

https://doi.org/10.1021/acs.macromol.1c00792
Macromolecules 2021, 54, 8936–8945

As shown in Figure 2b, the subsequent cooling from the micellar liquid phase to 200 °C induced micellar ordering into the HCP lattice. The (0002) peak was relatively weak due to small N_L and was hence masked by the $(10\bar{1}1)$ peak, such that the principal diffraction region appeared to be composed of two instead of three peaks (see Figure S3 of the Supporting Information for demonstration of the effect of N_L on the SAXS pattern). The $(10\bar{1}2)$ peaks in the SAXS profiles at both 200 and 180 °C were sharp, showing that the HCP phase developed at higher temperatures did not contain a significant population of stacking faults. Interestingly, the $(10\bar{1}2)$ peak broadened and diminished progressively with a further decrease in temperature, which was a manifestation of the increasing degree of stacking fault in the HCP regime. The $(10\bar{1}2)$ peak almost vanished at 30 °C, and the entire SAXS profile resembled that associated with the r-HCP phase (see Figure 1), indicating that the stacking fault was so abundant that the close-stacking sequence was nearly random. The temperature-dependent SAXS profiles in Figure 2b clearly demonstrated the presence of stacking faults in the HCP phase, and the degree of stacking fault increased with reducing temperature.

The sample having been cooled to 30 °C was reheated to examine if the variation of the degree of stacking fault was thermally reversible. Figure 2c displays the temperature-dependent SAXS profiles collected in the reheating cycle. It can be seen that, though the change was not as pronounced as that found in the cooling cycle, the $(10\bar{1}2)$ peak became stronger and sharper at higher temperature, signaling that the stacking fault was progressively removed upon heating. The subsequent recooling cycle displayed in Figure 2d shows identical temperature dependence of the scattering pattern to that found in the first cooling cycle (i.e., Figure 2b). The SAXS results in Figure 2 thus disclosed a thermally reversible variation of the degree of stacking fault, where the randomness of the close stacking of HCPLs in the HCP regime increased with decreasing temperature.

We attempted to estimate the values of α at different temperatures in the HCP regime by obtaining the SAXS profiles resembling the observed ones via calculating the scattering curves with assumed values of α using the Debye equation. In addition to the probability factor α, other variables considered in the calculation included N_L, N_p, the close stacking distance (i.e., $d_{(0002)}$), and the radius of the core, R_c. Figure 3 displays the representative comparison between the calculated and observed SAXS profiles collected in the cooling cycle. It is noted that our scattering model did not consider the other factors that also contribute to peak broadening, including the distributions of micelle size and interparticle distance as well as the lattice distortion from the fluctuations of particle positions. Although the calculated scattering curves fitted the experimental SAXS profiles reasonably well, as shown in Figure 3, the values of α thus obtained were considered as the first order of approximation for semiquantitative interpretation of the results.

Figure 4 plots the estimated values of α against temperature in the HCP regime. Consistent with the qualitative judgment from the intensity and width of the $(10\bar{1}2)$ peak, α was found to increase monotonically with decreasing temperature, meaning an increase in the degree of stacking fault in the HCP regime upon cooling. The change in α with temperature showed quite strong hysteresis; for instance, the value of α at 180 °C attained upon cooling from the micellar liquid phase

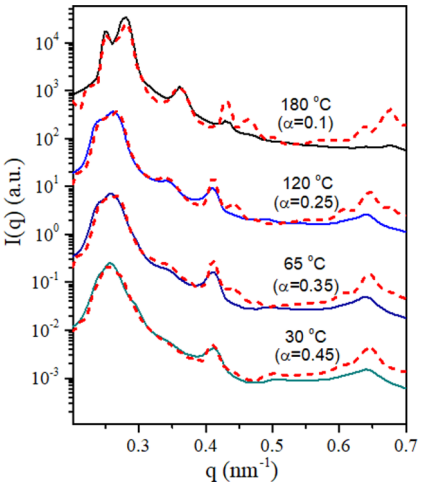

Figure 3. Fittings of the observed SAXS profiles at various temperatures in the cooling cycle for PEO-*b*-PB/h-PB blend (f_{PEO} = 0.20). The dashed line represents the calculated curve. The values of α used for calculating the SAXS curves are indicated directly in the figure.

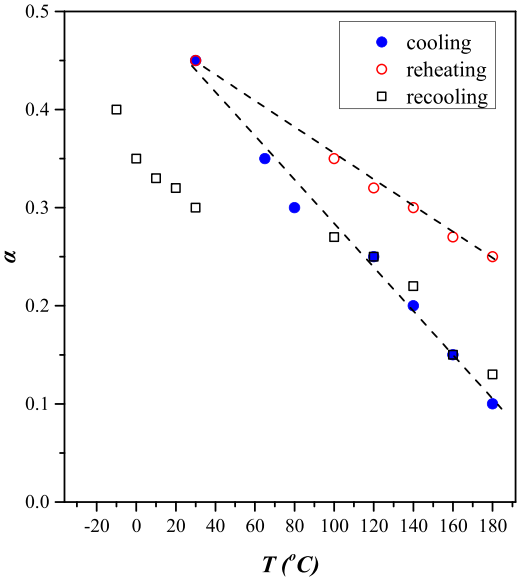

Figure 4. Temperature variation of the estimated value of α for the PEO-*b*-PB/h-PB blend (f_{PEO} = 0.20) in the cooling, reheating, and recooling cycle. The value of α was found to increase with decreasing temperature, showing the increase in the degree of stacking fault.

was ca. 0.1, whereas it was about 0.25 upon stepwise reheating to this temperature from 30 °C. We did not attempt to anneal such a reheated sample at 180 °C to examine if the stacking fault would be progressively removed due to the concern of thermal degradation. Nevertheless, Figure 4 demonstrated that the trend of the temperature variation of α was thermally reversible, i.e., α tended to decrease with decreasing temperature, in spite of the obvious hysteresis effect.

The effect of temperature on the degree of stacking fault in the HCP regime was also operative in the PEO-*b*-PB/h-PB blends with other compositions (see Figure S4 of the Supporting Information) and also in the PEO-rich blend (i.e., PEO-*b*-PB/h-PEO blend; see Figures S5 and S6 of the Supporting Information), where decreasing the temperature

https://doi.org/10.1021/acs.macromol.1c00792
Macromolecules 2021, 54, 8936−8945

amplified the degree of randomness of the close stacking of HCPLs.

The Thermodynamic Origin of the Temperature-Dependent Degree of Stacking Fault. The SAXS results of both PEO- and PB-rich blends revealed that the micelle ordering from the high-temperature micellar liquid phase upon cooling yielded HCP packing. The HCP phase thus formed contained stacking faults and their amount increased with decreasing temperature in a thermally reversible manner. The stacking fault of the close-packed lattices of metal atoms in metallic crystals can be created during crystal growth, during plastic deformation as partial dislocations move as a result of dissociation of a perfect dislocation, or by condensation of point defects during high-rate plastic deformation.[42] Stacking faults have also been found prevalently in hard-colloid crystals, where the r-HCP phase trapped in the freshly grown colloidal crystal transformed into the stable FCC phase with prolonged aging.[33,34,36] In both systems, the presence of stacking faults increases the free energy of the crystal, so the fault is not expected to recover once it is removed. The present study, however, showed that the micelles formed by the blends of a bcp with its corresponding homopolymers behaved differently in that the degree of stacking fault varied with temperature reversibly. It may be conjectured that the increase of the probability parameter α in the cooling process was due to the tendency of the HCP phase to transform into FCC packing via a mechanism accompanied with a continuous increase in α. To evaluate the possibility of such a mechanism, an isothermal annealing experiment was performed for the blend having been cooled to 30 °C for collecting the time-resolved SAXS profiles during the annealing process. It can be seen from Figure 5 that the SAXS profile, particularly the intensity and breadth of the $(10\bar{1}2)$ peak, was essentially unperturbed, showing no sign of progressive transformation to the FCC phase during the annealing process.

Another possible origin of the variation of the degree of stacking fault was relevant to the effect of temperature on micelle size. The stronger interblock repulsion at the lower temperature tends to increase the average size of the core microdomain (and hence micelle size) to reduce the surface-to-volume ratio of the core and hence the interfacial free energy. The increase of domain size is accomplished by the redistribution of the association number of the micelles that may involve micelle fusion and fission and even the diffusion of the bcp and homopolymer molecules. The micelles with renewed size then have to adjust their positions to fit in the HCP lattice with a larger unit cell. As the relocation of the micelles could involve cooperative micellar motion, which becomes more sluggish for larger micelles at lower temperature, the HCPLs might be trapped into false positions in the process of reorganization, leading to stacking faults in the HCP lattice.

Figure S7 of the Supporting Information displays the variation of the average radius of the PEO microdomain with temperature for the f_{PEO}/0.2 blend, showing that the core radius increased with decreasing temperature but tended to level off below 150 °C, while the degree of stacking fault still increased obviously (as demonstrated in Figure 4). The results showed that there was no distinct correlation between the fault probability α and micelle size. This argument is consolidated in Figure 6, displaying the overlay plots of the SAXS profiles collected at two temperatures for the two blend samples. It can be seen that the intensity profiles at $q > 0.5$ nm^{-1}, which were dominated by the form factor of the core domain, were essentially superimposable, whereas the intensity and breadth of the $(10\bar{1}2)$ peak were clearly different at the two temperatures, confirming that there was no definitive correlation between the degree of stacking fault and micelle size. As a result, the conjecture that the introduction of stacking faults arose from the misalignment of the HCPLs due to enlargement of micelle size upon decreasing temperature was precluded.

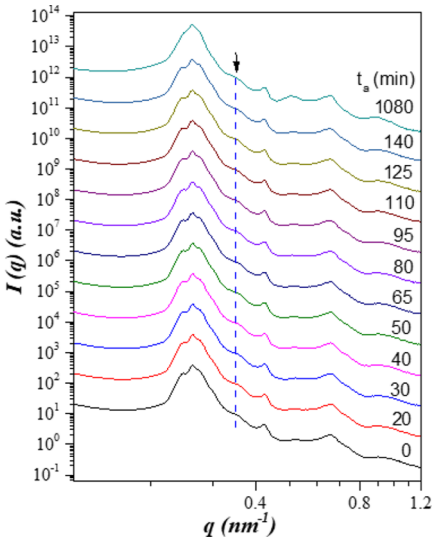

Figure 5. Time-resolved SAXS profiles collected during annealing at 30 °C for a PEO-*b*-PB/h-PB blend with f_{PEO} = 0.2. The intensity and breadth of the $(10\bar{1}2)$ peak pinpointed by the arrow were essentially unperturbed, showing that the close-packed structure did not progressively transform to the FCC phase during the annealing process.

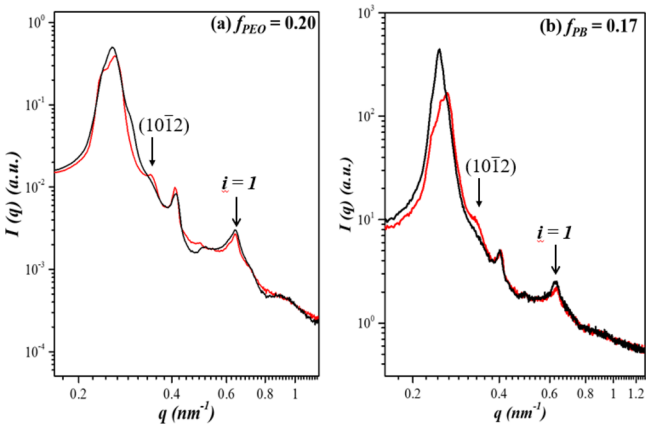

Figure 6. SAXS profiles collected at two temperatures for the two blend systems: (a) PEO-*b*-PB/h-PB blend with f_{PEO} = 0.20 at 120 °C (red curve) and 30 °C (black curve) and (b) PEO-*b*-PB/h-PEO blend with f_{PB} = 0.17 at 140 °C (red curve) and 100 °C (black curve). The peak marked by "i = 1" corresponds to the first-order form factor maximum of the PEO core domain. It can be seen that the intensity profiles at $q > 0.5$ nm^{-1}, which were dominated by the form factor of the core, were essentially superimposable, whereas the intensity and breadth of the $(10\bar{1}2)$ peak were different at the two temperatures, showing that there was no definitive correlation between the degree of stacking fault and micelle size.

https://doi.org/10.1021/acs.macromol.1c00792
Macromolecules 2021, 54, 8936−8945

The SAXS profiles observed experimentally corresponded to the ensemble average over a large number of grains in which the stacking fault was inserted statistically into the HCP lattice. In this case, the stacking sequence of the HCPL may vary from grain to grain, such that the close-packed structure was characterized by a large number of microstates with different stacking sequences, which was in clear contrast with the FCC and HCP phases wherein the sequences are fixed. The existence of numerous microstates leads to an increase in entropy relative to the HCP phase arising from the combinatorial arrangement of the positions of HCPLs along the stacking direction. In this regard, the introduction of stacking faults could be a thermodynamic requirement to minimize the free energy of the system. Here, we proceed with a thermodynamic analysis along this direction to show that the introduction of the stacking fault can indeed be thermodynamically driven.

Let us consider a single grain of the close-packed phase formed by the close stacking of N_L HCPLs with each layer comprising N_p particles. For the stacking sequence of three consecutive layers, i.e., $(i-1)$, (i), and $(i+1)$, if layers $(i-1)$ and $(i+1)$ adopt different positions (e.g., A and C, respectively), the sequence corresponds to an FCC unit, so layer (i) is denoted as an FCC layer. If layers $(i-1)$ and $(i+1)$ adopt the same position, layer (i) is assigned as an HCP layer. Once the stacking fault is inserted statistically, the probability α would represent the number fraction of the FCC layer and $(1-\alpha)$ is that of the HCP layer. Consequently, the bulk free energy of the close-packed structure is given by

$$F_{\text{bulk}} = N_p N_L[\alpha f_{\text{FCC}} + (1-\alpha) f_{\text{HCP}}] \tag{2}$$

where the product N_pN_L represents the total number of particles in the ordered phase and f_{FCC} and f_{HCP} are the bulk free energy per particle of the perfect FCC and HCP lattices, respectively. The free energy arising from the combinatorial mixing of FCC and HCP layers along the stacking direction is given by

$$F_{\text{mix}} = N_L k_B T[\alpha \ln \alpha + (1-\alpha)\ln(1-\alpha)] \tag{3}$$

According to Pronk and Frenkel,[33] there is also an interfacial free energy contributed by the interaction between an FCC layer and its adjacent HCP layer at the FCC−HCP boundary, which is expressed as

$$F_{\text{int}} = N_L \gamma_{\text{FH}} s_L \alpha(1-\alpha) \tag{4}$$

where γ_{FH} and s_L are the surface free energy per unit area and the surface area of an HCPL, respectively. It is noted that both F_{mix} and F_{int} are proportional to the total number of layers in the grain. Under a given total number of particles, the crystal with larger lateral dimension (or larger N_p) of the HCPL has fewer layers and hence a smaller contribution of F_{mix} and F_{int}.

Combining the three free-energy components followed by dividing the sum by the total number of particles (i.e., N_pN_L), we obtain the free-energy difference per particle between the close-packed structure containing the stacking fault and the perfect HCP lattice as follows

$$\begin{aligned}\Delta f(\alpha) &= f(\alpha) - f_{\text{HCP}} \\ &= \alpha \Delta f_{\text{FH}} + \frac{k_B T}{N_p}[\alpha \ln \alpha + (1-\alpha)\ln(1-\alpha)] \\ &\quad + \gamma_{\text{FH}} s_p \alpha(1-\alpha)\end{aligned} \tag{5}$$

where $\Delta f_{\text{FH}} = f_{\text{FCC}} - f_{\text{HCP}}$ is the difference in bulk lattice free energy per particle between the FCC and HCP phases and s_p is the contact area per particle at the FCC−HCP layer boundary.

According to the lattice-switch Monte Carlo simulation of hard-sphere colloid,[33] the HCP−FCC surface free energy $\gamma_{\text{FH}}s_p$ is extremely small, around $26 \times 10^{-5} k_B T$ per particle. We hence neglected this free-energy contribution and obtained the optimal stacking probability α_{op} of the finite-size crystal by minimizing the free energy via $\frac{\partial \Delta f(\alpha)}{\partial \alpha} = 0$. Hence, α_{op} is given by

$$\alpha_{\text{op}} = (1 + e^{(N_p \Delta f_{\text{FH}})/k_B T})^{-1} \tag{6}$$

The reason that the stacking probability given by eq 6 is the optimal instead of the equilibrium value is that the free energy given by eq 5 is not for an equilibrium crystal with infinitely large size but for a metastable equilibrium crystal with finite size. Equation 6 demonstrates that the optimal stacking probability is governed by the lateral size of the HCPL (prescribed by N_p) and Δf_{FH}, where the product $N_p\Delta f_{\text{FH}}$ signifies the difference in lattice free energy per HCPL. The Δf_{FH} of a hard-sphere crystal is of the order of $-10^{-3} k_B T$. Taking this order of magnitude into account, it can be shown that α_{op} approaches an asymptotic value of 1.0 (corresponding to the pure FCC lattice) at large N_p, whereas it approaches 0.5 (corresponding to r-HCP) when N_p is sufficiently small (see Figure S8 of the Supporting Information). Stable close-packed structures with α_{op} lying between 0.5 and 1.0 could form for intermediate crystal size. As a consequence, while FCC is the thermodynamically stable packing lattice for the equilibrium hard-sphere crystal, stacking faults with various degrees may be introduced favorably into an FCC crystal in practice due to small crystal size.

In the case of block copolymer micelles, the effect of crystal size or grain size on the stabilities of the close-packed lattices was first revealed by Chen *et al.* in a recent study of the micellar aqueous solution of poly(ethylene oxide)-*block*-poly(1,2-butdadiene).[39] The micelles composed of PB blocks in the core and the mixture of PEO blocks and water in corona were found to pack in the HCP lattice at the beginning of crystallization from the supercooled micellar liquid, as the small grain of the ordered phase gave rise to non-negligible Laplace pressure stabilizing the HCP packing. The HCP phase transformed into r-HCP and eventually to the thermodynamically stable FCC phase as the grain grew in size during crystallization. In a later study of the same micellar aqueous solution with a higher polymer concentration, Chen *et al.* further disclosed that the orthorhombic grain of a kinetically trapped FCC phase generated by mechanical shearing promoted the transition from FCC to the thermodynamically stable HCP phase via a martensitic shear transformation process.[40] In the FCC grains with orthorhombic-like geometry, the specific HCPLs dislocated for the martensitic shear transformation had the smallest cross-sectional areas and hence prescribed the lowest kinetic energy barrier for the diffusionless transformation.[40] These findings along with our thermodynamic analysis leading to eq 6 demonstrated that the structural characteristics of the grain of the ordered phase may exert a decisive effect on the experimentally observed close-packed structure particularly when the free-energy differences among the close-packed lattices are very small.

Δf_{FH} is positive for the PEO-*b*-PB/homopolymer blends;[43] therefore, α_{op} is expected to increase with decreasing N_p and

https://doi.org/10.1021/acs.macromol.1c00792
Macromolecules 2021, 54, 8936−8945

Δf_{FH} according to eq 6. That is, the increase of the extent of stacking fault with decreasing temperature could stem from the reduction of the lateral dimension of the HCPL and/or Δf_{FH}. The accurate determination of the N_p from fitting the experimental SAXS profiles was not plausible due to the inadequacy of our scattering model. Nevertheless, we found that the $(11\bar{2}0)$ peak was susceptible to the lateral dimension of the HCPL but not to the degree of stacking fault, where it diminished and broadened significantly with decreasing N_p (see Figure S3b of the Supporting Information), but remained virtually unperturbed with respect to the change in α under a fixed N_p (see Figure 1a). As a result, an examination of the effect of temperature on the intensity and breadth of this peak would allow the perturbation on N_p to be resolved. Figure S9 in the Supporting Information compares the intensity and breadth of the $(11\bar{2}0)$ peak in the SAXS profiles of the f_{PEO}/0.2 blend collected in the cooling cycle. It was found that, while the $(10\bar{1}2)$ peak broadened and diminished progressively with decreasing temperature, the $(11\bar{2}0)$ peak remained virtually unperturbed, signifying that the lateral grain size of the ordered phase largely preserved through the introduction of stacking faults.

In light of the fact that N_p was largely unperturbed by the change in temperature, the temperature-dependent degree of stacking fault observed here must arise from the reduction of Δf_{FH} with decreasing temperature, that is, the difference in bulk free energy between FCC and HCP lattices of the bcp micelles became smaller at lower temperature. According to the fundamental thermodynamic relationship

$$\left(\frac{\partial \Delta f_{FH}}{\partial T}\right) = -\Delta s_{FH} = s_{HCP} - s_{FCC}$$

where Δs_{FH} is the difference in entropy between FCC and HCP lattices per particle, the positive sign of $(\partial \Delta f_{FH}/\partial T)$ attests that the micelles packed in the HCP lattice have higher entropy than those organized in the FCC lattice, that is, HCP is an entropically favored close-packed structure for bcp micelles, though the origin of Δs_{FH} is not clear.

The fact that the thermally reversible variation of the degree of stacking fault was operative for bcp micelles but not in the previously studied hard-sphere crystals could be attributed to the small size and softness of the micelles. Bcp micelles are of a few tens of nanometers in diameter compared to hundreds of nanometers for hard colloids. The much smaller size and softness of the micelles allow them to diffuse more easily and collectively to adjust the positions of the HCPL for attaining the desired degree of stacking fault.

It is further noted that the blend systems studied here are composed of a homopolymer solubilized in the coronal region of the micelle; it is not clear if the variation of the degree of stacking fault with temperature would also occur in the corresponding neat bcp. According to our theoretical argument, Δf_{FH} is a key factor governing the degree of stacking fault, where lower Δf_{FH} favors the introduction of more stacking faults into the HCP phase. In the case of the bcp/homopolymer blend, the solubilization of the homopolymer introduces a negative free energy of mixing but the swelling of the coronal block by the homopolymer increases its conformational free energy. As a result, the Δf_{FH} of the blend could be different from that of the corresponding neat bcp due to these free-energy perturbations. We are currently studying if the temperature-dependent extent of stacking fault is also operative in sphere-forming PEO-*b*-PB. Suppression of this phenomenon in neat bcp would imply a larger Δf_{FH} or the grater difference in the thermodynamic stability between FCC and HCP lattices of the micelles formed by neat bcp molecules.

CONCLUSIONS

In summary, the HCP phase of the micelles formed in the blends of a bcp with its corresponding homopolymers exhibited a thermally reversible variation of the degree of stacking fault, where the population of the faulty layers increased with decreasing temperature. The stacking fault was considered to be thermodynamic in origin, as its presence contributes to the positive combinatorial entropy of mixing between HCP and FCC layers, which may compensate for the lattice free-energy penalty of inserting the faulty layers. If the penalty in lattice free energy is high (i.e., $\Delta f_{FH} \gg 0$) or when the lateral dimension of the HCPL is large, a perfect HCP packing is favored. Since the Δf_{FH} of a bcp micelle is tiny and the grain size of the experimentally accessed ordered phase is usually small, the contribution of the free energy of mixing could become significant, so that the minimum free energy is attained with an optimal extent of the stacking fault. The temperature dependence of the extent of the stacking fault was attributed to the decrease of the difference in bulk free energy between FCC and HCP phases with decreasing temperature, which further signified that the micelles packed in the HCP lattice have higher entropy than those organized in the FCC phase.

ASSOCIATED CONTENT

Supporting Information

The Supporting Information is available free of charge at https://pubs.acs.org/doi/10.1021/acs.macromol.1c00792.

> Molecular characterizations of the PEO-*b*-PB sample by gel permeation chromatography (GPC) and ^{1}H nuclear magnetic resonance (NMR) spectroscopy; detailed information of the compositions of the PEO-*b*-PB/homopolymer blends studied; calculated SAXS profiles of the HCP phase with systematic variations of the number of particles per HCPL (N_p) and the number of close-stacked layers (N_L); temperature-dependent SAXS profiles of other PEO-*b*-PB/h-PB blends showing an increase in the degree of stacking fault with decreasing temperature; temperature variation of the degree of stacking fault in PEO-*b*-PB/h-PEO blend; the variation of the average radius of the PEO core domain with temperature; the variation of the optimal stacking probability α_{op} for hard-sphere crystal calculated using eq 6; and the examination of the effect of temperature on the intensity and breadth of the $(11\bar{2}0)$ peak (PDF)

AUTHOR INFORMATION

Corresponding Author

Hsin-Lung Chen − *Department of Chemical Engineering, National Tsing Hua University, Hsinchu 30013, Taiwan;* orcid.org/0000-0002-3572-723X; Email: hlchen@che.nthu.edu.tw

Authors

Li-Ting Chen − *Department of Chemical Engineering, National Tsing Hua University, Hsinchu 30013, Taiwan*

https://doi.org/10.1021/acs.macromol.1c00792
Macromolecules 2021, 54, 8936−8945

Yu-Ting Huang − *Department of Chemical Engineering, National Tsing Hua University, Hsinchu 30013, Taiwan*
Chun-Yu Chen − *Experimental Facility Division, National Synchrotron Radiation Research Center, Hsinchu 30076, Taiwan*
Meng-Zhe Chen − *Department of Chemical Engineering, National Tsing Hua University, Hsinchu 30013, Taiwan*

Complete contact information is available at: https://pubs.acs.org/10.1021/acs.macromol.1c00792

Notes

The authors declare no competing financial interest.

■ ACKNOWLEDGMENTS

This work is supported by the Ministry of Science and Technology (MOST), Taiwan, under grant no. MOST 108-2221-E-007-021. The authors appreciate the beamtime of BL23A1 provided by NSRRC in Taiwan.

■ REFERENCES

(1) Frenkel, D. Order through entropy. *Nat. Mater.* **2015**, *14*, 9−12.
(2) Kittel, C.; McEuen, P.; McEuen, P. *Introduction to solid state physics*; 8th ed.; Wiley: New York, 2004.
(3) Frenkel, D.; Ladd, A. J. C. New Monte Carlo method to compute the free energy of arbitrary solids. Application to the fcc and hcp phases of hard spheres. *J. Chem. Phys.* **1984**, *81*, 3188−3193.
(4) Woodcock, L. V. Entropy difference between the face-centred cubic and hexagonal close-packed crystal structures. *Nature* **1997**, *385*, 141−143.
(5) Mau, S.-C.; Huse, D. A. Stacking entropy of hard-sphere crystals. *Phys. Rev. E* **1999**, *59*, 4396−4401.
(6) Thomas, E. L.; Kinning, D. J.; Alward, D. B.; Henkee, C. S. Ordered packing arrangements of spherical micelles of diblock copolymers in two and three dimensions. *Macromolecules* **1987**, *20*, 2934−2939.
(7) Grason, G. M. The packing of soft materials: Molecular asymmetry, geometric frustration and optimal lattices in block copolymer melts. *Phys. Rep.* **2006**, *433*, 1−64.
(8) Reddy, A.; Buckley, M. B.; Arora, A.; Bates, F. S.; Dorfman, K. D.; Grason, G. M. Stable Frank−Kasper phases of self-assembled, soft matter spheres. *Proc. Natl. Acad. Sci. U. S. A.* **2018**, *115*, 10233−10238.
(9) Lodge, T. P.; Bang, J.; Park, M. J.; Char, K. Origin of the thermoreversible fcc-bcc transition in block copolymer solutions. *Phys. Rev. Lett.* **2004**, *92*, 145501.
(10) Lodge, T. P.; Pudil, B.; Hanley, K. J. The full phase behavior for block copolymers in solvents of varying selectivity. *Macromolecules* **2002**, *35*, 4707−4717.
(11) Liu, Y.; Nie, H.; Bansil, R.; Steinhart, M.; Bang, J.; Lodge, T. P. Kinetics of disorder-to-fcc phase transition via an intermediate bcc state. *Phys. Rev. E* **2006**, *73*, 061803.
(12) Huang, Y.-Y.; Chen, H.-L.; Hashimoto, T. Face-centered cubic lattice of spherical micelles in block copolymer/homopolymer blends. *Macromolecules* **2003**, *36*, 764−770.
(13) Imaizumi, K.; Ono, T.; Kota, T.; Okamoto, S.; Sakurai, S. Transformation of cubic symmetry for spherical microdomains from face-centred to body-centred cubic upon uniaxial elongation in an elastomeric triblock copolymer. *J. Appl. Crystallogr.* **2003**, *36*, 976−981.
(14) Huang, Y.-Y.; Hsu, J.-Y.; Chen, H.-L.; Hashimoto, T. Precursor-Driven Bcc−Fcc Order−Order Transition of Sphere-Forming Block Copolymer/Homopolymer Blend. *Macromolecules* **2007**, *40*, 3700−3707.
(15) Huang, Y.-Y.; Hsu, J.-Y.; Chen, H.-L.; Hashimoto, T. Existence of fcc-packed spherical micelles in diblock copolymer melt. *Macromolecules* **2007**, *40*, 406−409.
(16) Chen, L.-T.; Chen, C.-Y.; Chen, H.-L. FCC or HCP: The stable close-packed lattice of crystallographically equivalent spherical micelles in block copolymer/homopolymer blend. *Polymer* **2019**, *169*, 131−137.
(17) Hsu, N.-W.; Nouri, B.; Chen, L.-T.; Chen, H.-L. Hexagonal Close-Packed Sphere Phase of Conformationally Symmetric Block Copolymer. *Macromolecules* **2020**, *53*, 9665−9675.
(18) Takagi, H.; Yamamoto, K. Close-packed structures of the spherical microdomains in block copolymer−homopolymer binary mixture. *Trans. Mater. Res. Soc. Jpn.* **2018**, *43*, 161−165.
(19) Takagi, H.; Hashimoto, R.; Igarashi, N.; Kishimoto, S.; Yamamoto, K. Synchrotron SAXS Studies on Lattice Structure of Spherical Micelles in Binary Mixtures of Block Copolymers and Homopolymers. *J. Fiber Sci. Technol.* **2018**, *74*, 10−16.
(20) Lee, S.; Bluemle, M. J.; Bates, F. S. Discovery of a Frank-Kasper σ phase in sphere-forming block copolymer melts. *Science* **2010**, *330*, 349−353.
(21) Lee, S.; Leighton, C.; Bates, F. S. Sphericity and symmetry breaking in the formation of Frank−Kasper phases from one component materials. *Proc. Natl. Acad. Sci. U. S. A.* **2014**, *111*, 17723−17731.
(22) Kim, K.; Schulze, M. W.; Arora, A.; Lewis, R. M., III; Hillmyer, M. A.; Dorfman, K. D.; Bates, F. S. Thermal processing of diblock copolymer melts mimics metallurgy. *Science* **2017**, *356*, 520−523.
(23) Schulze, M. W.; Lewis, R. M., III; Lettow, J. H.; Hickey, R. J.; Gillard, T. M.; Hillmyer, M. A.; Bates, F. S. Conformational asymmetry and quasicrystal approximants in linear diblock copolymers. *Phys. Rev. Lett.* **2017**, *118*, 207801.
(24) Li, W.; Duan, C.; Shi, A. C. Nonclassical spherical packing phases self-assembled from AB-type block copolymers. *ACS Macro Lett.* **2017**, *6*, 1257−1262.
(25) Kim, K.; Arora, A.; Lewis, R. M., III; Liu, M.; Li, W.; Shi, A.-C.; Dorfman, K. D.; Bates, F. S. Origins of low-symmetry phases in asymmetric diblock copolymer melts. *Proc. Natl. Acad. Sci. U. S. A.* **2018**, *115*, 847−854.
(26) Jeon, S.; Jun, T.; Jo, S.; Ahn, H.; Lee, S.; Lee, B.; Ryu, D. Y. Frank−Kasper Phases Identified in PDMS-b-PTFEA Copolymers with High Conformational Asymmetry. *Macromol. Rapid Commun.* **2019**, *40*, 1900259.
(27) Takagi, H.; Yamamoto, K. Phase Boundary of Frank−Kasper σ Phase in Phase Diagrams of Binary Mixtures of Block Copolymers and Homopolymers. *Macromolecules* **2019**, *52*, 2007−2014.
(28) Lachmayr, K. K.; Wentz, C. M.; Sita, L. R. An exceptionally stable and scalable sugar−polyolefin Frank−Kasper A15 phase. *Angew. Chem.* **2020**, *59*, 1521−1526.
(29) Yamamoto, K.; Takagi, H. Frank-Kasper σ and A-15 Phases Formed in Symmetry and Asymmetry Block Copolymer Blend System. *Mater. Trans.* **2021**, *62*, 325−328.
(30) Xie, J.; Shi, A.-C. Formation of complex spherical packing phases in diblock copolymer/homopolymer blends. *Giant* **2021**, *5*, 100043.
(31) Pusey, P. N.; Van Megen, W.; Bartlett, P.; Ackerson, B. J.; Rarity, J. G.; Underwood, S. M. Structure of crystals of hard colloidal spheres. *Phys. Rev. Lett.* **1989**, *63*, 2753−2756.
(32) Verhaegh, N. A. M.; van Duijneveldt, J. S.; van Blaaderen, A.; Lekkerkerker, H. N. W. Direct observation of stacking disorder in a colloidal crystal. *J. Chem. Phys.* **1995**, *102*, 1416−1421.
(33) Pronk, S.; Frenkel, D. Can stacking faults in hard-sphere crystals anneal out spontaneously? *J. Chem. Phys.* **1999**, *110*, 4589−4592.
(34) Kegel, W. K.; Dhont, J. K. G. "Aging" of the structure of crystals of hard colloidal spheres. *J. Chem. Phys.* **2000**, *112*, 3431−3436.
(35) Hoogenboom, J. P.; Derks, D.; Vergeer, P.; van Blaaderen, A. Stacking faults in colloidal crystals grown by sedimentation. *J. Chem. Phys.* **2002**, *117*, 11320−11328.
(36) Martelozzo, V. C.; Schofield, A. B.; Poon, W. C. K.; Pusey, P. N. Structural aging of crystals of hard-sphere colloids. *Phys. Rev. E* **2002**, *66*, 021408.

(37) Dolbnya, I. P.; Petukhov, A. V.; Aarts, D. G. A. L.; Vroege, G. J.; Lekkerkerker, H. N. W. Coexistence of rhcp and fcc phases in hard-sphere colloidal crystals. *Europhys. Lett.* **2005**, *72*, 962−968.
(38) Auer, S.; Frenkel, D. Prediction of absolute crystal-nucleation rate in hard-sphere colloids. *Nature* **2001**, *409*, 1020−1023.
(39) Chen, L.; Lee, H. S.; Lee, S. Close-packed block copolymer micelles induced by temperature quenching. *Proc. Natl. Acad. Sci. U. S. A.* **2018**, *115*, 7218−7223.
(40) Chen, L.; Lee, H. S.; Zhernenkov, M.; Lee, S. Martensitic transformation of close-packed polytypes of block copolymer micelles. *Macromolecules* **2019**, *52*, 6649−6661.
(41) Debye, P. Zerstreuung von röntgenstrahlen. Scattering from Non-Crystalline Substances. *Ann. Phys.* **1915**, *46*, 809−823.
(42) Li, B.; Yan, P. F.; Sui, M. L.; Ma, E. Transmission electron microscopy study of stacking faults and their interaction with pyramidal dislocations in deformed Mg. *Acta Mater.* **2010**, *58*, 173−179.
(43) Matsen, M. W. Fast and accurate SCFT calculations for periodic block-copolymer morphologies using the spectral method with Anderson mixing. *Eur. Phys. J. E* **2009**, *30*, 361−369.

https://doi.org/10.1021/acs.macromol.1c00792
Macromolecules 2021, 54, 8936−8945